Equilibrium high-temperature Fe isotope fractionation between fayalite and magnetite: An experimental calibration

Anat Shahar [a,*], Edward D. Young [a,b], Craig E. Manning [a]

[a] *Department of Earth & Space Sciences, University of California, Los Angeles, CA 90095 USA*
[b] *Institute of Geophysics and Planetary Physics, University of California, Los Angeles, CA 90095 USA*

Abstract

The iron isotopic fractionation factor between magnetite and fayalite was measured at high temperature in a piston–cylinder apparatus. For the first time, the three-isotope method [Matsuhisa, J., Goldsmith, J. R., and Clayton, R. N., 1978. Mechanisms of hydrothermal crystallisation of quartz at 250 °C and 15 kbar. Geochim. Cosmochim. Acta 42, 173–182.] has been used to determine equilibrium fractionation between two minerals directly. The experimentally-determined temperature-dependent iron isotope fractionation between fayalite and magnetite is described by $10^3 \ln \alpha^{57}_{Mag-Fa} \cong \Delta^{57}Fe_{Mag-Fa} = 0.30 \, (+/-0.024) \times 10^6 / T^2$. The equation predicts measurable fractionation at magmatic temperatures. Our work bears on the magnitude of Fe isotope fractionation attending differentiation in magmatic systems and provides a new isotope thermometer for co-existing fayalite and magnetite.
© 2008 Elsevier B.V. All rights reserved.

Keywords: iron isotope; thermometer; igneous rocks; high-temperature; three-isotope exchange; magnetite

1. Introduction

Iron isotope ratios have proven to be especially useful tracers in a variety of geochemical settings due to the ubiquitous nature of Fe and to its variable oxidation states. Differences in iron isotope ratios have been used to address a myriad of questions including, but not limited to, those relating to: biosignatures (Beard and Johnson, 1999), early solar system processes (Zhu et al., 2001), and planet formation processes (Poitrasson et al., 2004). Each of these applications depends critically on understanding factors that fractionate Fe isotopes.

Most work involving Fe isotopes has focused on low-temperature processes because differences between minerals equilibrated at high temperature are expected to be small due to decreasing fractionation with increasing temperature (T). But, with the advent of the multiple-collector inductively coupled plasma-source mass spectrometer (MC-ICPMS), these smaller differences in $\delta^{56}Fe$ and $\delta^{57}Fe$[1] can now be measured more precisely.

Differences between $\delta^{56(57)}Fe$ values of mantle minerals have been measured, but no consensus has been reached as to whether there are consistent iron isotopic fractionations amongst them. Zhu et al. (2002) found that olivine separates from lherzolites are isotopically lighter (by >0.2‰ in $^{57}Fe/^{54}Fe$) than co-existing orthopyroxene and clinopyroxene. Beard and Johnson (2004) found that olivine and orthopyroxene separates from spinel peridotites have indistinguishable $^{57}Fe/^{54}Fe$, whereas co-existing clinopyroxene and olivine were found to show some measurable differences in $\delta^{57}Fe$. A compilation of $\Delta^{56}Fe_{mineral-olivine}$ ($\Delta^{56}Fe_{i-j} = \delta^{56}Fe_i - \delta^{56}Fe_j$) representing separates of co-existing minerals in igneous rocks (Williams et al.,

* Corresponding author.
   E-mail address: ashahar@ess.ucla.edu (A. Shahar).

---

[1] $\delta^{56(57)}Fe = (^{56(57)}R_{smp} / ^{56(57)}R_{IRMM-014} - 1) * 1000$ where $^{56(57)}R = ^{56(57)}Fe/^{54}Fe$ and IRMM-014 is an international Fe standard. In what follows reference will be made to both $\delta^{56}Fe$ and $\delta^{57}Fe$ since both values are reported by various authors. In all cases considered here Fe isotope fractionation is mass dependent and so there is no significance to choosing one ratio over the other.

2005; Beard and Johnson, 2004; Zhu et al., 2002) is shown in Fig. 1. The plot underscores the fact that there are no clear systematic inter-mineral relationships emerging from the studies thus far. The peaks for the fractionations between olivine (Ol) and clinopyroxene (Cpx), orthopyroxene (Opx), spinel (Spl), and magnetite (Mag) all overlap, with no mineral defining a population that is clearly resolvable from olivine. Calculations of bond strength predict that magnetite and spinel should concentrate ^{56}Fe and ^{57}Fe relative to ^{54}Fe more than co-existing silicate minerals because of the lower Fe coordination in the spinel-group minerals (Polyakov and Mineev, 2000). Of the minerals presented in Fig. 1, magnetite should show the largest difference from olivine due to its crystal chemistry and yet the magnetite data are centered on $\Delta^{56}Fe_{Mag-Ol}=0$.

One explanation for a lack of a clear trend in Fig. 1 may be that differentiation processes are accompanied by Fe isotope fractionation, resulting in variable mineral $^{56}Fe/^{54}Fe$ values that reflect not only equilibrium mineral fractionation, but differences in bulk rock Fe isotope ratios from open-system processes. In the absence of direct experimental determination of Fe isotope fractionation factors it is not possible to determine what causes the lack of systematics among mantle igneous minerals shown in Fig. 1.

Understanding the equilibrium inter-mineral $^{57}Fe/^{54}Fe$ (and $^{56}Fe/^{54}Fe$) differences amongst high-temperature minerals should be valuable for interpretations of the significance of iron isotope ratios in igneous rocks, especially at the sub-‰ level currently being investigated. *Ab initio* predictions for Fe isotope fractionation among high-T minerals exist, but experiments will ultimately be required to verify predictions, and in some cases to supplant them. To date there have been just two published high-temperature iron isotope experimental studies. Roskosz et al. (2006) investigated the kinetic fractionation of iron isotopes between a silicate melt and metal alloys at high temperature and room pressure. Schuessler et al. (2007) reported the iron isotopic fractionation factor between pyrrhotite and silicate melt at high pressure and temperature.
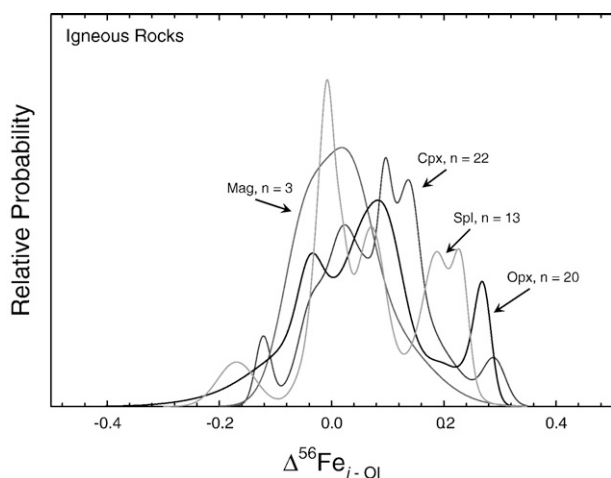
In this study we use the three-isotope exchange method (originally used for oxygen by Matsuhisa et al., 1978) to experimentally determine the equilibrium iron isotope fractionation factor between fayalite and magnetite as a function of temperature in the assemblage magnetite + quartz + fayalite (Fa) comprising the "QFM" oxygen fugacity buffer. This study is a first step in experimentally quantifying inter-mineral Fe isotope fractionation in natural samples at high temperatures and known oxygen fugacity. Our results demonstrate that igneous differentiation involving magnetite, and by extension other spinel phases with tetrahedrally coordinated Fe, can result in shifts in igneous rock Fe isotope ratios. They also provide a well-calibrated Fe isotope thermometer for magnetite-fayalite-bearing rocks in equilibrium.

2. Methods

2.1. Piston–cylinder experiments

Starting materials were finely ground powders of synthetic, high-purity fayalite, quartz, and hematite. The fayalite and quartz were synthesized hydrothermally. Hematite was prepared by mixing α-Fe_2O_3 powder (Alfa Aesar) with high-purity α-$^{54}Fe_2O_3$ (Oak Ridge National Laboratory Batch 154891, ^{54}Fe 98.37%, ^{56}Fe 1.55%, ^{57}Fe 0.07%, ^{58}Fe 0.008%) in a 99:1 ratio. The mixture was twice ground under acetone in a mortar and pestle for 30 min. The starting mineral assemblage which consisted of ~50 mg of synthetic fayalite and quartz and ~10 mg of hematite, was ground for 20 min under acetone to produce a homogeneous mixture.

For each experiment the starting assemblage was loaded with ~15 mg nanopure H_2O into segments of Au tubing of 3.5 mm outer-diameter and 0.18 mm wall thickness. The capsule was then welded shut and checked for leaks by heating at 100 °C for 30 min and checking for weight loss. Any capsule that lost weight was incompletely sealed and discarded.

All experiments were performed in a 1-inch diameter piston–cylinder apparatus with NaCl pressure medium and graphite heater sleeve. A thin piece of Au was placed on top of the capsule to prevent puncture by the thermocouple. Temperature was monitored with $Pt/Pt_{90}Rh_{10}$ thermocouples in contact with the capsule, with no correction for the effect of pressure on emf. The accuracy of the reported temperature is estimated to be ±3 °C. All experiments were brought to a pressure of 7 kbar and then heated to the desired run temperature, where thermal expansion of the assembly brought the pressure to 10 kbar. Pressure was monitored with a Heise gauge and maintained to within 200 bar gauge pressure. Experiments were quenched by cutting power to the apparatus, which resulted in cooling of the experiment to <50 °C in <1 min (Manning and Boettcher, 1994).

Following each run, the capsules were retrieved, cleaned, and pierced with a needle, releasing water through the hole. The presence of water indicated that the capsule did not leak during the experiment. The run products were then carefully removed and placed in a glass container. After optical inspection using a binocular microscope, magnetite and fayalite were separated

Fig. 1. Relative probability plot showing $\Delta^{56}Fe_{mineral-olivine}$ in natural igneous rocks. Data compiled from Williams et al. (2005), Beard and Johnson (2004), and Zhu et al. (2002).

with a hand magnet. The fayalite was purified by handpicking to a purity of ~100% and the magnetite was picked to a purity of >98%.

2.2. MC-ICPMS analyses

Experimental products were dissolved in a mixture of hydrofluoric and nitric acids. The solution was then dried down on a hot plate and dissolved again in hydrochloric and nitric acids to make sure dissolution was complete, and then dried again on a hot plate. The final iron solution was picked up in 2% nitric acid for introduction into the mass spectrometer.

All Fe isotope ratio measurements were made using a ThermoFinnigan Neptune MC-ICPMS. The instrument has a fixed array of 9 Faraday collectors each with amplifier resistors of 10^{11} Ω. Mass interferences from ArO^+ (~2.5 mV), $ArOH^+$ (<1 mV), and ArN^+ (~1.8 V) were resolved from $^{56}Fe^+$, $^{57}Fe^+$ and $^{54}Fe^+$, respectively, by operating at a high mass resolving power of $m/\Delta m > 10{,}000$ (Weyer and Schwieters, 2003). Corrections for instrumental mass bias were obtained by using sample-standard bracketing with peak height matching between sample and standard to better than 5%. Sample and standard were analyzed as ~5 ppm Fe in 2% HNO_3 aspirated through a Cetac Aridus desolvating nebulizer (samples were run in dry plasma). Samples were analyzed 8 to 10 times with each analysis consisting of 20 cycles of ~4 second integrations. The starting solutions were checked for $^{52}Cr^+$ and in each case the intensity was found to be less than 2 mV, which was taken to indicate that $^{54}Cr^+$ interference for $^{54}Fe^+$ was negligible. The purity of the solutions obviated the need for purification of Fe; potential instrumental mass bias due to inter-element matrix effects was not an issue for these pure solutions containing the analyte Fe. In this study it is the relative differences in Fe isotope ratios that are of interest. We use the international Fe isotope standard IRMM-014 as a primary standard in our laboratory, but because we are concerned with relative differences we did not exchange secondary standards with other laboratories as part of this work.

2.3. Three-isotope exchange method

In order to establish that our measured fractionation factors represent equilibrium, we used the three-isotope exchange method first described by Matsuhisa et al. (1978). In that study and in those following, fractionation factors between a mineral and water were obtained by adding an isotope spike to one of the reactants. To our knowledge, our study is the first to employ the three-isotope technique to determine an inter-mineral equilibrium fractionation factor directly.

In the context of three Fe isotopes a condition for equilibrium between two phases i and j is $\alpha_{i-j}^{56/54} = \left(\alpha_{i-j}^{57/54} \right)^{\gamma}$ where $\alpha_{i-j}^{56/54} = {}^{56}R_i / {}^{56}R_j$ and the exponent γ relating the three isotopes at equilibrium is

$$\gamma = \frac{\frac{1}{m_{56}} - \frac{1}{m_{54}}}{\frac{1}{m_{57}} - \frac{1}{m_{54}}}, \tag{1}$$

where m is the mass of subscripted Fe isotope. In this case $\gamma = 0.67795$. The exponent γ is effectively the slope of a fractionation line on a plot of $\delta^{56}Fe$ vs. $\delta^{57}Fe$ since $\delta^{56}Fe_i - \delta^{56}Fe_j \sim 10^3 \ln \alpha_{i-j}^{56/54}$ and $\delta^{57}Fe_i - \delta^{57}Fe_j \sim \gamma 10^3 \ln \alpha_{i-j}^{56/54}$. Over the range of isotopic fractionations discussed in this paper these approximations impart only a ppm level of error that is well within analytical uncertainties, e.g. Young et al. (2002).

The principle of the three-isotope exchange method is to replace the terrestrial fractionation line (TFL) having a zero intercept with a secondary fractionation line (SFL) that has a non-zero intercept by use of a spike (Fig. 2). The secondary fractionation line will have the same slope as the TFL but will be displaced from it in proportion to the amount of spike. The equation

$$\delta^{56}Fe_i = \gamma \delta^{57}Fe_i + \left(\delta^{56}Fe_o - \gamma \delta^{57}Fe_o \right) \tag{2}$$

relates the equilibrium Fe isotope ratios for phase i on the SFL where $\delta^{56}Fe_o$ and $\delta^{57}Fe_o$ are the δ values for the total Fe comprising the spiked experimental system. The last term in Eq. (2) is the intercept on the Fe three-isotope plot (Fig. 2). At isotopic equilibrium all phases containing Fe must lie on the SFL defined by Eq. (2). The bulk composition of the experimental system, described by $\delta^{56}Fe_o$ and $\delta^{57}Fe_o$, therefore depends on the initial iron fractions of fayalite and spiked hematite.

A series of experiments at a single temperature can fail to yield isotopic equilibrium. In this circumstance the compositions of each partially equilibrated phase, representing varying extents of exchange reaction, will define a straight line extending from the starting composition toward the equilibrium composition on the SFL (Fig. 2). Extrapolation of each line to its intersection with the SFL therefore defines the equilibrium isotopic compositions for the phases of interest. The three-isotope method is thus an especially powerful tool at lower temperatures, where kinetics are slower and equilibrium is seldom attained.
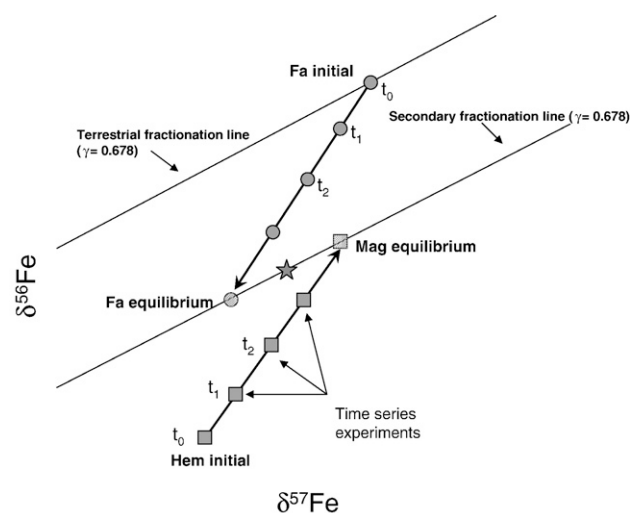

Fig. 2. Schematic diagram of the three-isotope exchange method showing the terrestrial fractionation line (TFL) where all natural samples lie, the secondary fractionation line which has the same slope as the TFL but is offset from the TFL due to a ^{54}Fe spike, and a series of experiments with trajectories that intersect the secondary fractionation line. The intersections of the trend lines from the experiments and the secondary fractionation line define the equilibrium isotopic compositions.

Utilization of the three-isotope method to determine equilibrium fractionations between mineral pairs in the presence of a solvent requires that the minerals do not completely dissolve and then reprecipitate. This is because reprecipitation from a homogeneous medium such as a fluid or melt could yield mineral pairs lying on an SFL but not in exchange equilibrium. This potential problem was avoided in our experiments because the volume of H_2O present in the capsules was relatively small and mineral solubilities are extremely low at our run conditions. For example, magnetite solubility in H_2O at 800 °C and 10 kbar is extremely low, even in the presence of NaCl (Wykes et al., in press).

A second requirement of the three-isotope method is that no metaphases are present in the runs used to define the equilibrium fractionation factor. Our use of hematite as a starting material thus hinges on complete conversion to magnetite during experiments. Accordingly, we carefully checked all runs to confirm that no hematite was present.

2.4. Analytical errors and their propagation

Uncertainties in $\Delta^{57}Fe_{Mag-Fa}$ reported in this study are derived from isotope ratio measurements of fayalite and magnetite from a series of experiments. The method of propagating the uncertainties in individual analyses to the final equilibrium $\Delta^{57}Fe_{Mag-Fa}$ is described below.

The uncertainty in each isotope ratio measurement is the standard error of 8 to 10 analyses of the same sample solution. Analyses of a given mineral for experimental runs of different duration but the same temperature (e.g., 4 analyses of magnetite for experiments at 800 °C) are regressed using the "new" York

regression (Mahon, 1996). Once a regression and associated uncertainties in slope and intercept are obtained for all magnetite and fayalite products for a given temperature, the equilibrium $\Delta^{57}Fe_{Mag-Fa} = \delta^{57}Fe_{Mag} - \delta^{57}Fe_{Fa}$ for that temperature is obtained from the difference in the intersection of the magnetite and fayalite regression lines with the secondary fractionation line in three-isotope space. Intersections of $\delta^{57}Fe$ values are calculated from slopes and intercepts according to the relation

$$\delta^{57}Fe_{Eq,i} = \frac{-b_1 + b_2}{m_1 - \gamma} \qquad (3)$$

where $\delta_i{}^{57}Fe_{Eq,i}$ is the projected $\delta^{57}Fe$ value for mineral i at equilibrium, m_1 is the slope of the regressed data points for mineral i, γ is the slope of the secondary fractionation line, b_1 is the intercept of the best-fit line through the regressed data points, and b_2 is the intercept of the secondary fractionation line. Uncertainties in the derived $\Delta^{57}Fe_{Mag-Fa}$ values are obtained from the intersections of the 95% confidence error envelopes (Ludwig, 1980) for the magnetite and fayalite best-fit lines and the secondary fractionation line. The $\delta^{57}Fe$ values for the intersection of the SFL and the 95% confidence error envelope for each best-fit line is calculated using the expression

$$\delta^{57}_{95\%-SFL} = \Big(\pm \big(\sigma_{m_1}^4 \overline{\delta^{57^2}} + 2\sigma_{m_1}^2 \overline{\delta^{57}} (\gamma - m_1)(b_2 - b_1) \qquad (4)$$
$$+ \gamma^2 \sigma_{b_1}^2 - 2\gamma \sigma_{b_1}^2 m_1 + b_2^2 \sigma_{m_1}^2 - 2b_2 b_1 \sigma_{m_1}^2$$
$$+ b_1^2 \sigma_{m_1}^2 + \sigma_{b_1}^2 (m_1^2 - \sigma_{m_1}^2) \big)^{1/2} - \sigma_{m_1}^2 \overline{\delta^{57}}$$
$$+ (\gamma - m_1)(b_1 - b_2) \Big) / \gamma^2 - 2\gamma m_1 - \sigma_{m_1}^2 + m_1^2$$

where $\delta^{57}_{95\%-SFL}$ is the $\delta^{57}Fe$ value for the intersection of the 95% envelope and the SFL (+/− accounts for the two boundaries of the

Table 1
Experimental results

Name	Mineral	Temp (°C)	Time (h)	$\delta^{56}Fe$ (‰)	$\delta^{57}Fe$ (‰)	$\delta^{56}Fe$	% Exchange *
Start	Fayalite	–	–	0.64(1)	0.95(6)	0.00	–
Start	Hematite	–	–	−12.63(4)	−12.32(7)	−4.29	–
Start	Hematite3	–	–	−11.13(2)	−10.75(3)	−3.85	–
Start	Hematite4	–	–	−10.88(1)	−10.57(1)	−3.72	–
QFM18	Fayalite	600	24	−0.04(1)	0.21(2)	−0.19	25
QFM18	Magnetite	600	24	−3.29(2)	−2.93(3)	−1.30	82
QFM21	Fayalite	600	48	−1.01(2)	−0.77(3)	−0.49	45
QFM21	Magnetite	600	48	−4.60(2)	−4.32(2)	−1.68	79
QFM22	Fayalite	600	73	−0.97(1)	−0.73(2)	−0.48	51
QFM22	Magnetite	600	73	−3.76(1)	−3.44(2)	−1.41	83
QFM23	Fayalite	700	24	−1.75(1)	−1.49(1)	−0.74	65
QFM23	Magnetite	700	24	−4.04(1)	−3.71(1)	−1.52	85
QFM24	Fayalite	700	48	−0.88(1)	−0.62(2)	−0.46	46
QFM24	Magnetite	700	48	−4.15(1)	−3.84(2)	−1.55	80
QFM25	Fayalite	700	72	−1.68(1)	−1.45(2)	−0.70	65
QFM25	Magnetite	700	72	−3.80(1)	−3.47(1)	−1.45	86
QFM12	Fayalite	800	6	−0.88(2)	−0.61(3)	−0.47	48
QFM12	Magnetite	800	6	−4.63(2)	−4.31(2)	−1.51	82
QFM13	Fayalite	800	12	−1.33(1)	−1.08(2)	−0.60	78
QFM13	Magnetite	800	12	−2.58(2)	−2.25(2)	−0.93	95
QFM10	Fayalite	800	24	−2.26(2)	−1.99(4)	−0.91	94
QFM10	Magnetite	800	24	−2.53(2)	−2.20(4)	−1.04	98
QFM8	Fayalite	800	49	−2.37(2)	−2.11(3)	−0.93	100
QFM8	Magnetite	800	49	−2.12(2)	−1.76(4)	−0.92	100

* Percent exchange $((\delta - \delta_0)/(\delta_{eq} - \delta_0)*100)$ refers to the degree at which the mineral has come to equilibrium in the particular experiment. It is not reproducible and depends on experimental conditions.

envelope) , σ_{b1} is the uncertainty (se) in b_1, σ_{m1} is the uncertainty in m_1, and $\overline{\delta^{57}}$ is the centroid δ^{57}Fe value for the regressed data. Standard errors for the equilibrium δ^{57}Fe values for magnetite and fayalite obtained by extrapolation are calculated by dividing the 95% uncertainties in intersections by 2 (assuming 95% confidence limits are ~2 se). These standard errors for the equilibrium δ^{57}Fe$_{Mag}$ and δ^{57}Fe$_{Fa}$ values are then propagated through to the final Δ^{57}Fe$_{Mag-Fa}$ in the usual way (square root of sum of squares). The standard errors reported below for the Δ^{57}Fe$_{Mag-Fa}$ at each temperature were determined in this manner (reported as 2 se). Finally, the values of Δ^{57}Fe$_{Mag-Fa}$ at each temperature were regressed (Mahon, 1996) in order to obtain the final equation for the temperature dependence of Δ^{57}Fe$_{Mag-Fa}$ with associated uncertainty.

3. Results

Results of the experiments at 600 °C, 700 °C and 800 °C are given in Table 1, along with the starting compositions of the hematite and fayalite. Each isothermal set of experiments was conducted with a new batch of spiked hematite standard, leading to different hematite starting compositions. The experiments at 700 °C and 800 °C were conducted at 10 kbar. At 600 °C the pressure was dropped to 9.5 kbar to ensure fayalite+quartz stability relative to ferrosilite (Bohlen et al., 1980).

3.1. Textures

Product mineral assemblages and textures were examined by optical microscopy and scanning electron microscopy (SEM). Fayalite, magnetite and quartz were the only minerals present in the run products. No evidence for hematite was found during optical inspection at low magnification. SEM petrography (Fig. 3) showed that magnetite occurs in all run products as fine-grained (~1–2 μm) matted clusters of octahedra interspersed between fayalite and quartz. Quartz recrystallized to large (~10–30 μm) equant crystals. Fayalite forms intermediate (~5–10 μm) sub-hedral prisms. The run-product textures therefore suggest that conversion of hematite to magnetite occurred rapidly (<6 h). Comparison of run products from the 800 °C experiments of 6 and 48 h duration (Fig. 3a, b) revealed similar textures and grain sizes, indicating insignificant grain annealing or textural modification from 6 to 48 h, perhaps owing to the relatively low mineral solubilities in H_2O. These observations establish that the equilibrium mineral assemblage was rapidly attained in all experiments. As discussed below, isotopic exchange equilibrium among these phases occurred more slowly, highlighting the utility of the three-isotope method in establishing equilibrium in piston–cylinder experiments.

3.2. 800 °C

Experiments were performed at 800 °C (Fig. 4a, b) for 6, 12, 24, and 49 h. Fayalite and magnetite from the 49 h run lie on the SFL for this temperature in three-isotope space (Fig. 4), indicating close approach to exchange equilibrium. The inferred equilibrium Δ^{57}Fe$_{Mag-Fa}$ at 800 °C is 0.28 +/− 0.04‰ (2 se). Fig. 5 shows the
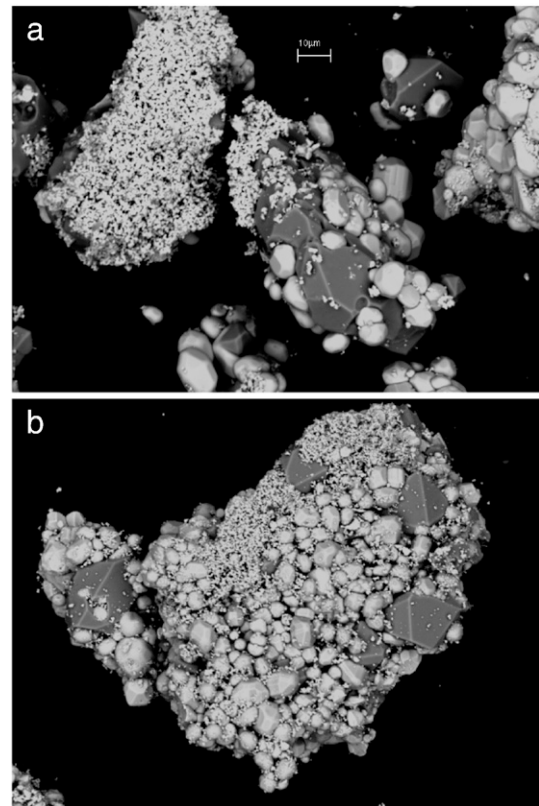

Fig. 3. Backscattered electron images showing the crystal faces and textures of experimental run products grown at 800 °C for 6 h (a) and 48 h (b). The largest crystals are quartz (dark grey), followed by fayalite (light grey) and then magnetite (white). The scale bar is the same in both images.

secondary fractionation lines in detail at each temperature to highlight intersections with the 95% confidence error envelopes discussed above.

3.3. 700 °C and 600 °C

Experiments were performed at 700 °C (Fig. 4c, d) and 600 °C (Fig. 4e, f) for 24, 48, and ~72 h. None of these experiments attained isotopic equilibrium, as indicated by the fact that none of the experimental products at these temperatures have isotopic compositions on the secondary fractionation lines. The equilibrium Fe isotope ratios of magnetite and fayalite at these temperatures were therefore obtained by extrapolation to the respective SFLs. Extrapolation of the regressed data to the SFLs at each temperature yielded Δ^{57}Fe$_{Mag-Fa}$ values of 0.31 +/−0.08‰ at 700 °C and 0.38 +/−0.06‰ at 600 °C.

3.4. Temperature dependence of equilibrium Fe isotope exchange

The experimentally-determined magnetite–fayalite fractionations are plotted as a function of temperature in Fig. 6. The experimental values are compared to the theoretical curves for olivine and magnetite fractionation from Polyakov and Mineev (2000), Polyakov et al. (2007), and Mineev et al. (2007). When
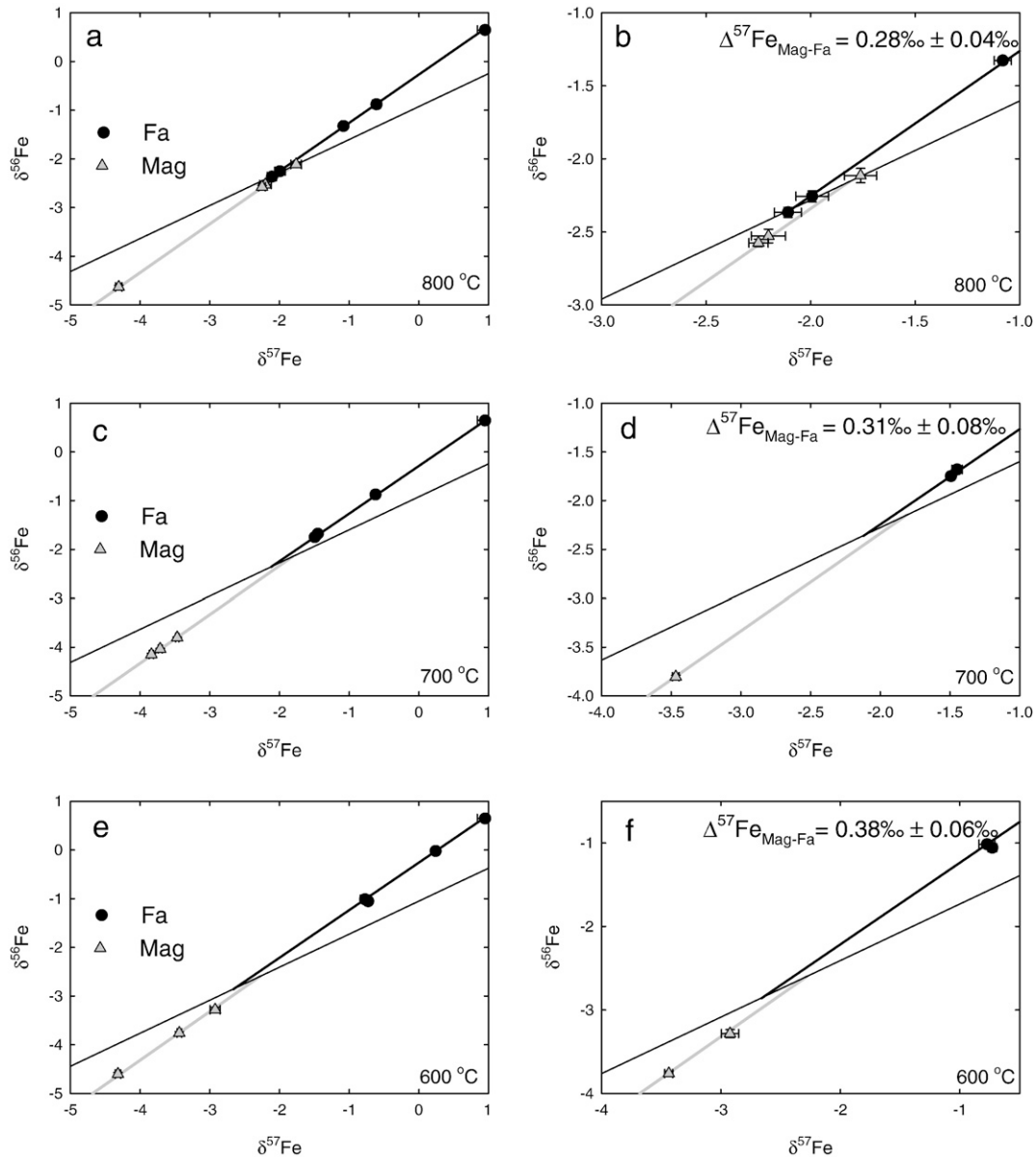
Fig. 4. Experimental results at 800 °C (a, b), 700 °C (c, d), and 600 °C (e, f). Fig. 4b, d, and f are close-ups of a, c, and e respectively. The black circles are fayalite, and the gray triangles are magnetite. The minerals at 800 °C have come to equilibrium on a secondary fractionation line determined by the bulk Fe isotopic composition of the system. Error bars (2 se) are shown where they are larger than symbol sizes. The best-fit line was calculated using the new York regression (Mahon, 1996). See text for more details.

the data are regressed (Mahon, 1996) by forcing the best-fit line through the origin, the temperature-dependence of the magnetite–fayalite fractionation factor is

$$\Delta^{57}\text{Fe}_{\text{Mag–Fa}} = 0.30(+/-0.024) \times 10^6/T^2 \tag{5}$$

where the uncertainty is at the 2 se level.

4. Discussion

4.1. Comparison to theoretical predictions

Recent theoretical studies have predicted the magnitude and direction of iron isotopic fractionation between various phases

and molecules at a range of temperatures. Equilibrium isotopic fractionations are caused by sensitivities of vibrational frequencies to isotopic substitutions. The vibrational frequencies for modes of vibration in a material can be calculated with first-principles quantum mechanical methods (e.g., Jarzecki et al., 2004). Alternatively, Mössbauer spectroscopy or Inelastic Nuclear Resonant X-ray Scattering (INRXS) can be used to obtain vibrational properties of ^{57}Fe within minerals, and then the vibrational frequencies for other isotopes can be calculated (e.g., Polyakov and Mineev, 2000). The theoretical predictions can be extended over a range of temperature conditions so as to give the theoretical fractionation factor for two minerals as a function of temperature. These predictions come in the form of ratios of reduced (i.e., vibrational) partition function ratios for
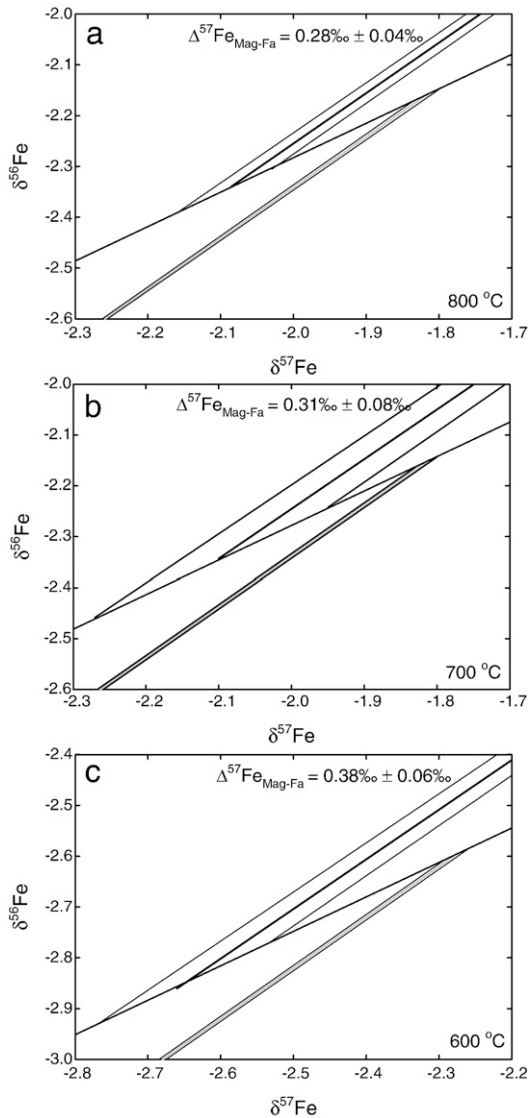
Fig. 5. Intersections between secondary fractionation lines and 95% confidence error envelopes for best fits to fayalite and magnetite data in Fe three-isotope space. Best-fit lines are shown for experiments performed at 800 °C (a), 700 °C (b), and 600 °C (c). Fits to fayalite are shown as heavy black lines. Fits to magnetite are shown as heavy grey lines. Error envelopes are shown as thinner lines. Data points are out of the field of view.

phases i, relative to some common reference state for the element of interest. These reduced partition function ratios β_i, also referred to as β-factors, define the fractionation factor according to the relation $\ln \alpha_{i-j} = \ln \beta_i - \ln \beta_j$ where α_{ij} is the equilibrium isotope fractionation factor between phases i and j.

The most important determining factor for $^{56}Fe/^{54}Fe$ (or $^{57}Fe/^{54}Fe$) fractionation is bond stiffness, because bond strengths determine vibrational frequencies that in turn determine internal energies. Higher oxidation state and lower coordination number will lead to stiffer bonds that concentrate heavy isotopes in order to minimize the total vibrational energy of the system. Fayalite, $Fe^{VI}_2Si^{IV}O_4$, incorporates only ferrous (Fe^{2+}) iron into its structure and always in octahedral coordination, whereas magnetite, $(Fe^{3+})^{IV}(Fe^{3+}Fe^{2+})^{VI}O_4$, incorporates both ferrous and ferric iron

into its structure, in a 1:2 ratio, and with half of the ferric iron in tetrahedral coordination. Therefore, the prediction is that magnetite in equilibrium with fayalite will concentrate more of the heavy isotope and have a greater $\delta^{57}Fe$ value than fayalite at equilibrium.

Polyakov and Mineev (2000) published β-factors for olivine and magnetite based on Mössbauer spectroscopy data. The authors predict an enrichment of heavy iron isotopes in Fe^{3+} bearing minerals. The β-factors for magnetite were recently revised (Polyakov et al., 2007; Mineev et al., 2007) in view of new INRXS data and new Mössbauer data. (The two studies differ due to slight differences in the oxidation state of Fe in the magnetite measured.) Our experimentally-determined temperature-dependent $\Delta^{57}Fe_{Mag-Fa}$ equation falls within a range defined by the two most recent theoretical studies (Fig. 6). The close match between the experimental results and the theoretical results is apparently due in part to the well-characterized differences in the crystal chemical environment of Fe in magnetite and fayalite.

4.2. Applications to natural systems

Recent work (Poitrasson and Freydier, 2005; Schoenberg and von Blanckenburg, 2006) has suggested that the most evolved magmas show the heaviest iron isotopic signatures. This trend towards high $^{57}Fe/^{54}Fe$ isotope compositions with magma evolution could be due to open-system behavior, late-stage fluid exsolution processes, or fractional crystallization. With the data presented in this study, it is possible to assess the direction and magnitude of changes in $\delta^{57}Fe$ attending differentiation by fractional crystallization if the fractionating assemblage includes a spinel phase (e.g., magnetite) because it is the difference in coordination between tetrahedral and octahedral Fe that drives the fractionation and Fe is likely to be octahedrally coordinated in silicate melts.

One can apply the equilibrium fractionation factor determined in this work to estimate Fe isotope fractionation attending fractional crystallization of magnetite by treating fractional crystallization as a Rayleigh process. Grove and Kinzler (1986) present a model for fractional crystallization of an andesitic lava with a fractionating assemblage that includes magnetite. Based
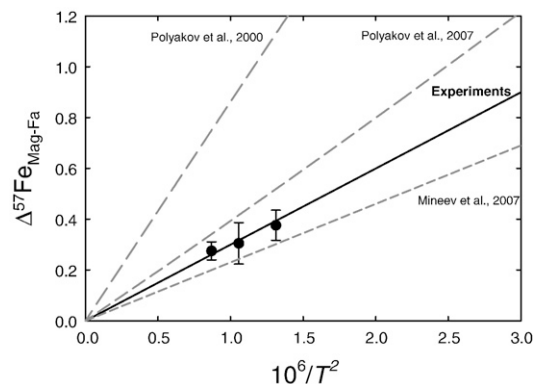

Fig. 6. Experimental magnetite–fayalite Fe isotope fractionation data plotted as a function of temperature along with theoretical predictions for the fractionation (see text). Error bars shown are 2 se.

on their model, approximately 80% of the Fe lost from the melt is extracted as magnetite. The relevant equation for Rayleigh fractionation is

$$^{57}R/^{57}R_i = F^{\alpha-1}, \tag{6}$$

where ^{57}R is the $^{57}Fe/^{54}Fe$ isotopic ratio of the remaining melt, $^{57}R_i$ represents the initial isotope ratio of the melt, F is the fraction of liquid remaining and $\alpha_{solid-melt}$ is the fractionation factor between fractionating solids and melt. Based on the model of Grove and Kinzler, F varies from 1 to ~0.33 for evolving andesite magmas when magnetite dominates the fractionating assemblage for Fe. For this simple calculation we use the fractionation between magnetite and fayalite as a model for the fractionation between magnetite and melt. Since 80% of the Fe fractionation occurs by magnetite removal, we dilute the magnetite–melt fractionation factor to simulate the bulk solid–melt fractionation factor. The dilution, whereby $\alpha_{solid-melt} = 0.8$ α_{Mag-Fa}, assumes all other fractionation factors between crystallizing Fe-bearing minerals and melt are unity. Fig. 7 shows that for temperatures of 1000 °C and 1100 °C an andesitic magma series affected by magnetite fractionation could exhibit shifts in $^{57}Fe/^{54}Fe$ of up to 0.27‰. This is a measurable amount of Fe isotope fractionation given the precision with which $^{57}Fe/^{54}Fe$ is measured by MC-ICPMS ($2\sigma < 0.05‰$).

The trend observed in the above simplistic model would predict that evolved magmas would become lighter during fractional crystallization if magnetite was a major fractionating phase. Since this is not what is observed in the literature to date, one concludes that magmatic differentiation in the rocks studied thus far did not occur by fractional crystallization of tetrahedrally coordinated Fe. Alternatives are that partial melting and/or metasomatic processes dominated the Fe isotope systematics (Williams et al., 2004).

Nonetheless, Fe isotopic signatures of magnetite fractionation should exist in differentiation sequences in which magnetite played an important role. Crystallization of magnetite is sensitive to the oxygen fugacity of the melts and under the right oxidation conditions, magnetite will be the dominant Fe-bearing fractionating phase. The Skaergaard Intrusion would provide a good test of the predicted decrease in $^{57}Fe/^{54}Fe$ with differentiation if the processes responsible for magnetite fractional crystallization occurred in quasistatic isotopic equilibrium and under closed-system conditions (e.g., Fig. 7). The differentiation sequence of the Skaergaard is thought to have been characterized by the appearance of magnetite in the final stages of differentiation (Hunter and Sparks, 1987). Magnetite crystallization strongly depleted the total Fe of the melt along a classical tholeiitic liquid line of descent. The crystallization temperature of magnetite is thought to be between 1000 °C and 1100 °C, suggesting that shifts in $\delta^{57}Fe$ in the Skaergaard sequence should be on the order of 0.2 to 0.3‰.

Fractionation of Fe isotopes between magnetite and fayalite could be a useful thermometer for rocks containing these minerals. The uncertainty in the temperature from this calibration is

$$\sigma_T = 500 \sqrt{\frac{\sigma_M^2}{\Delta_{Mag-Fa}^{57} M} + \frac{M \sigma_{\Delta_{Mag-Fa}^{57}}^2}{\left(\Delta_{Mag-Fa}^{57}\right)^3}} \tag{7}$$

where M is the calibration slope (0.30), σ_M is the standard error in the slope (+/−0.012), Δ_{Mag-Fa}^{57} is the *measured* fractionation, and $\sigma_{\Delta_{Mag-Fa}^{57}}$ is the uncertainty in the *measured* fractionation. Typical uncertainties in measured $^{57}Fe/^{54}Fe$ in minerals (e.g., +/−0.02‰ 2 se) suggest that the resolution of this technique would be on the order of ±40 °C (1 se) at magmatic temperatures. The thermometer has the advantage that it relies only on isotopic equilibrium between these two phases.

4.3. Oxygen fugacity

Although Fe oxidation state and oxygen fugacity are linked, there are complications in the simple statement that ferrous iron should be found in reduced environments and ferric iron in oxidized environments. Some minerals incorporate Fe^{3+} into their structures (e.g., spinel), while others will exclude Fe^{3+} even under highly oxidizing conditions (e.g., olivine). The differences in structures that accommodate ferrous iron or ferric iron are more complicated than the simple loss or gain of an electron. The addition of Fe^{3+} can replace a trivalent cation, such as Al, and many times requires a coupled substitution or the creation of defects. For these reasons, although the iron oxidation state in crystalline materials can be influenced by the overall environmental oxidation state, the relationship is apt to be less straightforward than in, for example, aqueous solutions or melts.

At each temperature in our experiments the oxygen fugacity is known since the stable assemblage in the runs comprise the quartz–fayalite–magnetite (QFM) oxygen fugacity buffer. Williams et al. (2004) presented iron isotope data for a suite of mantle minerals in an attempt to determine whether iron isotopic fractionation could be used as a tracer for changes in mantle oxidation state. The authors found lower $^{57}Fe/^{54}Fe$ for mantle spinels with higher oxygen fugacity and an inverse
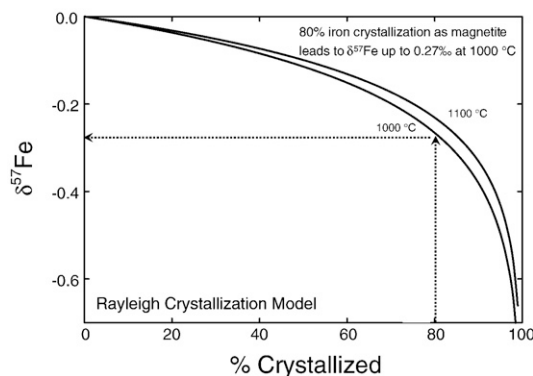

Fig. 7. Rayleigh fractionation model for Fe isotope fractionation attending differentiation of an andesite magma by fractional crystallization of magnetite. In this calculation 80% of the Fe present as solid is in the form of magnetite (see text). Using the experimental fractionation factor between fayalite and magnetite determined in this study as a proxy for silicate melt–magnetite fractionation, the prediction is that an andesite liquid line of descent will exhibit a change in $^{57}Fe/^{54}Fe$ of 0.27‰ at 1000 °C.

correlation between $^{57}Fe/^{54}Fe$ and Fe^{3+} concentration in spinel. These findings apparently contradict expectations based on bond strength; the expectation is that higher charged Fe^{3+} will result in stiffer bonds and therefore greater $^{57}Fe/^{54}Fe$. Williams et al. (2004) attribute their results to open-system processes. More experiments will be required to investigate Fe isotope fractionation involving spinels other than magnetite and the effect of oxygen fugacity on iron isotope fractionation in different geochemical settings.

5. Conclusions

This work shows that the three-isotope method is an effective means of establishing that isotopic equilibrium has been attained in a piston–cylinder experiment. Using this technique we find a temperature-dependent Fe isotope fractionation between fayalite and magnetite at magmatic and high-grade metamorphic temperatures that can be used as a quantitative thermometer in rocks containing these minerals. Agreement between the experimental result reported here and previous predictions based on *ab initio* calculations and spectroscopy validates our understanding of the underlying controls for Fe isotope fractionation in mineral phases. In particular, Fe isotope fractionation between magnetite and fayalite is relatively large because of the presence of Fe in tetrahedral coordination in magnetite. Changes in Fe isotope ratios are expected to be evident in magmatic differentiation sequences where magnetite was a fractionating phase. In order to understand the meaning of small but significant differences in Fe isotope ratios among minerals representing differentiated planetary materials (e.g., samples of Earth's mantle) the mechanisms of high-T Fe isotope fractionation must be quantified. The experimental approach taken here shows considerable promise for establishing equilibrium fractionation factors in high-T and high-P experiments.

Acknowledgements

References

Beard, B.L., Johnson, C.M., 2004. Inter-mineral Fe isotope variations in mantle-derived rocks and implications for the Fe geochemical cycle. Geochim. Cosmochim. Acta 68, 4727–4743.

Beard, B.L., Johnson, C.M., 1999. High precision iron isotope measurements of terrestrial and lunar materials. Geochim. Cosmochim. Acta 63, 1653–1660.

Bohlen, S.R., Essene, E.J., Boettcher, A.L., 1980. Reinvestigation and application of olivine–quartz–orthopyroxene barometry. Earth Planet. Sci. Lett. 47, 1–10.

Grove, T.L., Kinzler, R.J., 1986. Petrogenesis of andesites. Annu. Rev. Earth Planet. Sci. 14, 417–454.

Hunter, R.H., Sparks, R.S.J., 1987. The differentiation of the Skaergaard intrusion. Contrib. Mineral. Petrol. 95, 451–461.

Jarzecki, A.A., Anbar, A.D., Spiro, T.G., 2004. DFT analysis of Fe(H2O)(6)(3+) and Fe(H2O)(6)(2+) structure and vibrations; implications for isotope fractionation. J. Phys. Chem. A 108, 2726–2732.

Ludwig, K.R., 1980. Calculation of uncertainties of U–PB isotope data. Earth Planet. Sci. Lett. 46, 212–220.

Mahon, K.I., 1996. The new "York" regression: application of an improved statistical method to geochemistry. Int. Geol. Rev. 38, 293–303.

Manning, C.E., Boettcher, S.L., 1994. Rapid-quench hydrothermal experiments at mantle pressures and temperatures. Am. Mineral. 79, 1153–1158.

Matsuhisa, J., Goldsmith, J.R., Clayton, R.N., 1978. Mechanisms of hydrothermal crystallisation of quartz at 250 °C and 15 kbar. Geochim. Cosmochim. Acta 42, 173–182.

Mineev, S.D., Polyakov, V.B., Permyakov, Y.V., 2007. Equilibrium iron isotope fractionation factors for magnetite from Mössbauer spectroscopy and inelastic nuclear resonant X-ray scattering data. Geochim. Cosmochim. Acta 71 A669 Suppl.

Poitrasson, F., Freydier, R., 2005. Heavy iron isotope composition of granites determined by high resolution MC-ICP-MS. Chem. Geol. 222, 132–147.

Poitrasson, F., Halliday, A.N., Lee, D.C., Levasseur, S., Teutsch, N., 2004. Iron isotope differences between Earth, Moon, Mars and Vesta as possible records of contrasted accretion mechanisms. Earth Planet. Sci. Lett. 223, 253–266.

Polyakov, V.B., Clayton, R.N., Horita, J., Mineev, S.D., 2007. Equilibrium iron isotope fractionation factors of minerals: reevaluation from the data of nuclear inelastic resonant X-ray scattering and Mössbauer spectroscopy. Geochim. Cosmochim. Acta 71, 3833–3846.

Polyakov, V.B., Mineev, S.D., 2000. The use of Mössbauer spectroscopy in stable isotope geochemistry. Geochim. Cosmochim. Acta 64, 849–865.

Roskosz, M., Luais, B., Watson, H.C., Toplis, M.J., Alexander, C.M.O., Mysen, B.O., 2006. Experimental quantification of the fractionation of Fe isotopes during metal segregation from a silicate melt. Earth Planet. Sci. Lett. 248, 851–867.

Schoenberg, R., von Blanckenburg, F., 2006. Modes of planetary-scale Fe isotope fractionation. Earth Planet. Sci. Lett. 252, 342–359.

Schuessler, J.A., Schoenberg, R., Behrens, H., von Blanckenburg, F., 2007. The experimental calibration of the iron isotope fractionation factor between pyrrhotite and peralkaline rhyolitic melt. Geochim. Cosmochim. Acta 71, 417–433.

Weyer, S., Schwieters, J.B., 2003. High precision Fe isotope measurements with high mass resolution MC-ICPMS. Int. J. Mass Spectrom. 226, 355–368.

Williams, H.M., McCammon, C.A., Peslier, A.H., Halliday, A.N., Teutsch, N., Levasseur, S., Burg, J.P., 2004. Iron isotope fractionation and the oxygen fugacity of the mantle. Science 304, 1656–1659.

Williams, H.M., Peslier, A.H., McCammon, C., Halliday, A.N., Levasseur, S., Teutsch, N., Burg, J.P., 2005. Systematic iron isotope variations in mantle rocks and minerals: the effects of partial melting and oxygen fugacity. Earth Planet. Sci. Lett. 235, 435–452.

Wykes, J. L., Newton, R. C., and Manning, C. E., in press. Solubility of andradite, Ca3Fe2Si3O12, in a 10 mole % NaCl solution at 800 °C and 10 kbar: implications for the metasomatic origin of grandite garnet in skarns and calc–silicate granulites. American Mineralogist.

Young, E.D., Galy, A., Nagahara, H., 2002. Kinetic and equilibrium mass-dependent isotope fractionation laws in nature and their geochemical and cosmochemical significance. Geochim. Cosmochim. Acta 66, 1095–1104.

Zhu, X.K., Guo, Y., Williams, R.J.P., O'Nions, R.K., Matthews, A., Belshaw, N.S., Canters, G.W., de Waal, E.C., Weser, U., Burgess, B.K., Salvato, B., 2002. Mass fractionation processes of transition metal isotopes. Earth Planet. Sci. Lett. 200, 47–62.

Zhu, X.K., Guo, Y., O'Nions, R.K., Young, E.D., Ash, R.D., 2001. Isotopic homogeneity of iron in the solar nebula. Nature 412, 311–313.